Dereth Drake, Old Dominion University, Norfolk, VA; Svetozar Popovic, Old Dominion University, Norfolk, VA; Leposava Vuskovic, Old Dominion University, Norfolk, VA; Thao Dinh, Berriehill Research Corporation, Dayton, OH
AIAA-2010-1536
48th AIAA Aerospace Sciences Meeting Including the New Horizons Forum and Aerospace Exposition, Orlando, Florida, Jan. 4-7, 2010

Effects of Water Vapor Presence in Martian Atmospheric Entry Plasma

D. Janette Drake[1], Svetozar Popović[2], and Leposava Vušković[3]
Old Dominion University, Norfolk, VA 23529

Thao Dinh[4]
Berriehill Research Corp., Dayton, OH 45459

Effects of water vapor presence in Martian atmospheric entry plasma (MAEP) were calculated based on entry data from the Viking, Pathfinder, and the Mars Exploration Rover Opportunity Landers. Calculations of the temperature and electron density across the shock front were made. We employed steady state and non-steady state kinetic models to describe the rate of dissociation of CO_2 in the Martian atmosphere as well as the production of O_2. Water vapor was included in the models since it represents 0.03% of the surface atmospheric composition. With the addition of small amounts of water vapor, we found a decrease in the dissociation of CO_2 in the Martian air as well as an increase in the production of O_2.

I. Introduction

NASA's Mars exploration program seeks to understand Mars as a dynamic system, including measuring the structure of the upper atmosphere and ionosphere, understanding the past and present climate, and its potential habitability. In keeping with these goals, many satellites and landers have been sent to Mars [1]. Each of these Martian probes and satellites faced numerous challenges on their long missions. For the satellites, one the most challenging phases is the aerobraking phase. First used by the Magellan spacecraft while orbiting Venus in 1993 [2] and then by the Mars Global Surveyor in 1997 [3], the satellites skimmed the atmosphere of the planet using the friction between the atmosphere and the probes to slow their velocity. This subsequently led to a decrease in the orbital radius for the satellite. The major benefit of this process is that the naturally occurring forces were used to decrease the altitude of the orbit as opposed to a de-orbital burn which would involve the use of fuel to ignite the engines. Since less fuel was needed for the mission to get the satellite into orbit, the cost was lower. This friction also caused heating and ionization of the surrounding atmosphere, generating Martian atmospheric entry plasma (MAEP), which is relatively poorly understood.

Martian entry plasma is a complex mixture consisting of numerous atomic gases, molecular gases, ions, and electrons. Modeling of these types of plasmas is very computationally intensive. Gorelov *et al.* [4] showed, through a comparison of experiments and numerical simulations at shock speeds of 4-9 km/s, that to model this type of discharge a weaker dissociation rate for CO_2 molecules has to be included in the model. In addition, they showed that for non-equilibrium ionization behind the shock fronts a slower ionization rate for C and O atoms by electron

[1] Ph.D. student, Department of Physics
[2] Professor, Department of Physics, AIAA Member
[3] Professor, Department of Physics
[4] Research Scientist

impact and the non-equilibrium distribution of the free electron temperature must also be included. In an earlier work by Park *et al.* [5], a thermochemical model using the previously identified molecular, atomic, and ionic species was used to show that the vibrational temperature approaches the translational temperature quickly behind the shock front.

In recent years, there have been many models and experiments of CO_2/N_2 hypersonic flows in a convergent-divergent nozzle for application to Martian atmospheric entry [6]-[8]. Using a thermochemical non-equilibrium Navier-Stokes solver, these researchers have shown how the rotational temperature, vibrational temperature, number density, and molar fractions of the gases vary in a plasma arcjet under specific laboratory conditions. The main problem with these models and experiments is that they do not include argon as a key ionizing species in the discharges. In addition, they do not take into account the correct geometry for the Martian landers.

It has been known since the development of carbon dioxide lasers that small amounts of water (order of 100 ppm) reduce substantially its dissociation rates and improves life-time and efficiency of laser devices. We have proven that the dissociation of carbon dioxide in RF discharge can be reduced by 20% (*Thao Dinh etal* 1997) with addition of 100 ppm of water. These and higher quantities are naturally present in the Martian atmosphere, and their effect may be more important than it was assumed in previous models.

The goal of this paper is to study the kinetics MAEP and in particular the interactions of this type of plasma with the shock front which form in front of the Martian Landers, with the emphasis on the effects of impurities, water and OH radicals in particular. The paper is thus set up as follows: In section II we describe the entry trajectory data and the shock wave jump parameters for these probes as well as for the Mars Exploration Rovers (MER) Opportunity and Spirit. In section III we describe the electron energy distribution functions and the calculation of the electron density under jump conditions for three Martian probes given that the dominant neutral species in the MAEP will be CO_2, O_2, O, CO, NO, N_2, and Ar. We also discuss the seeding effect of residual electrons that have been measured in the upper Martian atmosphere In section IV we discuss the steady state and non-steady state gas composition of MAEP. Finally, in section V we discuss the inclusion of water vapor in the model and how it impacts the dissociation rate of CO_2 in the Martian atmosphere.

II. Martian Atmospheric Entry Characteristics and Shock Parameters

NASA's Pathfinder and Viking Landers found that the Martian atmosphere below 100km was primarily composed of CO_2 (95.32%) with minor components of N_2 (2.7%) and Ar (1.6%) [9]. In addition, these landers also observed the free stream density, pressure, and temperature during the entry phase into the atmosphere. This phase begins at approximately 180 km above the surface and lasts until the parachutes are deployed for landing, around 9 km, with a total elapsed time of approximately 120 s. The free stream temperature measurements from the Pathfinder Lander and Viking Landers 1 & 2 are presented in Fig. 1. From the figure, we observe that the temperature is very high in the upper atmosphere which most likely is caused by solar radiation. The temperature then decreases with decreasing altitude reaching a minimum at 80 km. According to Schofield *et al.* [10], this temperature minimum may be due to a superposition of waves, such as thermal tides. These tides will propagate from the lower atmosphere to higher altitudes with increasing amplitude. After 80 km the temperature once again begins to increase till it reaches an average of about 220 K at the surface.

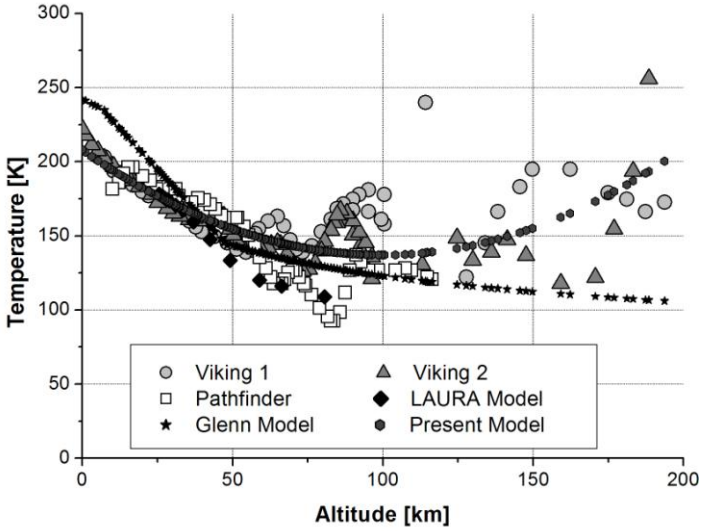

Fig. 1. Temperature distributions in the Martian atmosphere from Viking Landers 1 & 2, Pathfinder Lander, the Glenn model, input to LAURA model calculations, and our present model.

By reconstructing the entry trajectory of the Martian probes, when we use the present model we are able to develop an accurate portrait of all the atmospheric phenomena faced by them. For instance, Viking Lander trajectory at various stages covered latitudes between 15 and 22 degrees, approximately and longitudes between 300 and 310 degrees east. Mars Pathfinder landing site was at 23^{o}N and 338^{o}E. All landings were made during the daytime.

There is additional uncertainty posed by the latitudinal and longitundinal atmospheric conditions, by seasonal and diurnal variations of temperature, For instance, data from Thermal Emission Spectrometer (TES) suggest significant latitudinal dependence of free stream temperature as shown in Figure 2. Mean temperature at the longitude of 270^{o} during southern hemisphere summer show relatively uniform behavior up to about northern latitude of 30^{o}. Northern winter is presented by a substantial reduction of temperature above 30^{o}.

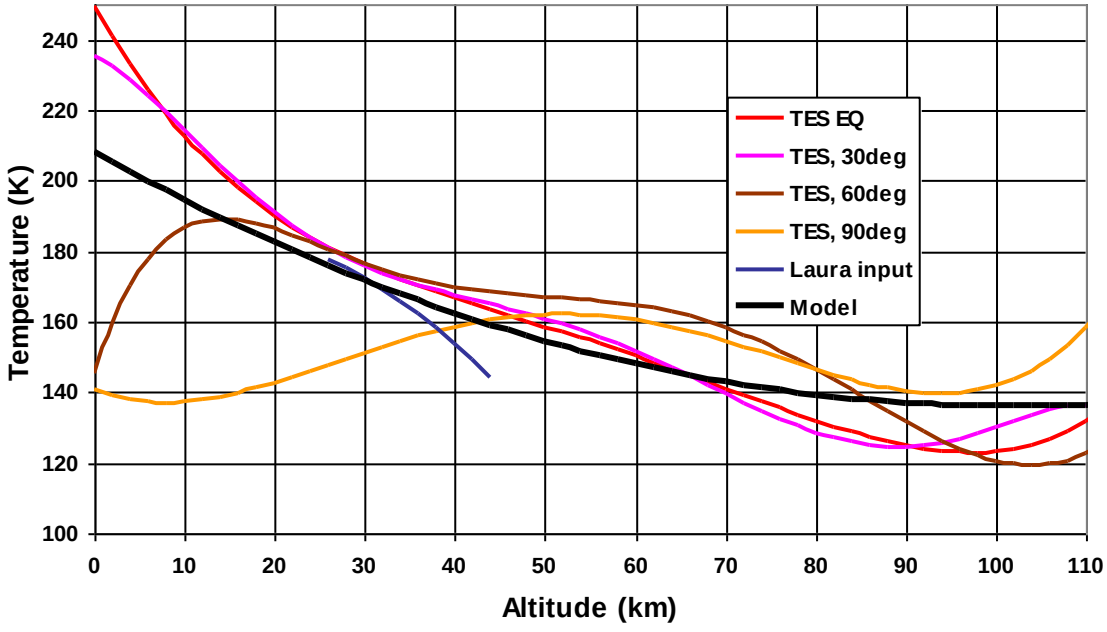

Fig. 2. Temperature distribution at various northern latitudes during the southern summer on Mars, according to TES data. Variations around equator are insignificant but they are large at higher latitudes. Present fitting model is averaged over larger altitude range, so that it deviates from measured data near surface by more than 10%.

The Mach number (M) for each probe was determined by using M = v/c_s, where v is the velocity of the probe and c_s is the speed of sound in the medium determined by

$$c_s = \sqrt{\frac{\gamma RT}{m_m}} \, . \tag{1}$$

Here γ is the specific heat ratio, R is the universal gas constant, m_m is the molecular mass, and T is the temperature from Fig. 1 and we present these results in Fig. 3. From the figure we observe that the Mach number increases as the probes enters the atmosphere with peak values of 42, 31, and 25 for the Pathfinder, MER Opportunity, and Viking Landers, respectively. Then the Mach number begins to decrease sharply due to an increase in atmospheric density.

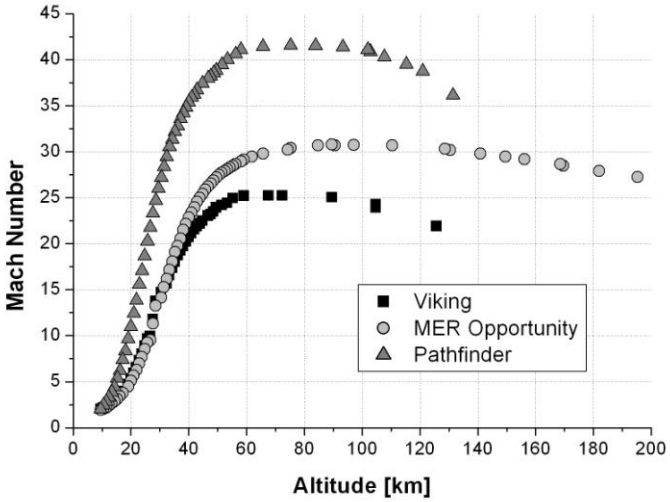

Fig. 3. Calculated values of the Mach number for the Viking, Pathfinder, and MER Opportunity Landers [11].

In order to accurately estimate electron density and gas composition for Martian atmospheric entry plasma (MAEP), we must construct a simple model for the shock region in front of each probe during entry. For this model certain assumptions must be made: (1) the gas mixtures generated during entry are thermodynamically perfect gases, (2) ionization occurs instantly behind the shock front, (3) the gas mixtures are constant in the boundary layer behind the shock front, and (4) gas parameters are defined by the free stream parameters and the relations across the shock. From these assumptions, we are able to calculate the shock parameters, such as the temperature,

$$T_2 = T\left\{1+\frac{2(\gamma-1)}{(\gamma+1)^2}\frac{\mathrm{A_M}-1}{\mathrm{A_M}}\left[\gamma \mathrm{A_M}+1\right]\right\} \, , \tag{2}$$

where $\mathrm{A_M} = \mathrm{M}(T)^2 \sin^2 \beta$, β is the oblique shock angle, and T is the atmospheric temperature from Fig. 1. Employing Eq. (2) we calculated the temperature across the shock front and present these results in Fig. 4. We observe that the temperature reaches a peak average value of about 36000 K, 19000 K, and 13000 K for the Pathfinder, MER Opportunity, and Viking Landers, respectively. These maximum values occurred between 50 and 60 km above the surface. The shaded regions give us a range of values for the temperature. For example, the Pathfinder Lander has a peak temperature of 36000 K ± 2500 around 60 km. At higher altitudes all the distributions become wider since the atmosphere becomes less dense. Uncertainty due to latitudinal variation of temperature is relatively low in the regions near equator, which reflects relatively minor error at low altitudes.

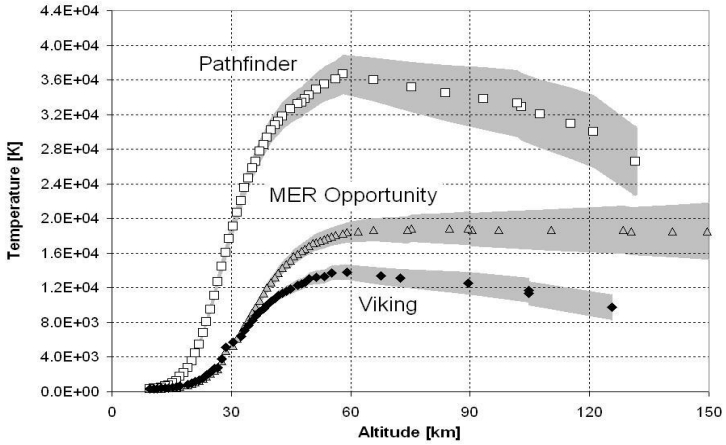

Fig. 4. Temperature across the shock layer in the MAEP. The shaded region is due to the uncertainties of the measured free stream temperature data [11, which reflect global and latitudinal variations of probe trajectories.

III. Evaluation of the Electron Energy Distribution Function and Electron Density

Martian air flow around the spacecraft can be divided into three distinct regions that have various level of equilibrium conditions. First, free atmosphere at high altitudes is known to be weakly ionized. In fact, spacecraft passes through a quite dense ionosphere, which extends above 300 km. Measured vertical electron and major ion density distribution in the altitude range above 100 km is shown in Figure 5. Most of ionization comes from solar UV radiation. This is confirmed by the fact that the peak electron density depends on solar zenith angle, and by strong observed diurnal variations. However, the ionosphere still exists in the dark side, and there a high level of ionization is seen even at large zenith angles (70-80^o). Explanations could include a possibility of large amount of energy stored by photo-excitation and cascade processes in the vibrationally and electronically excited states of O_2 and CO_2 and much stronger ionizing radiation activity in the diluted atmosphere.

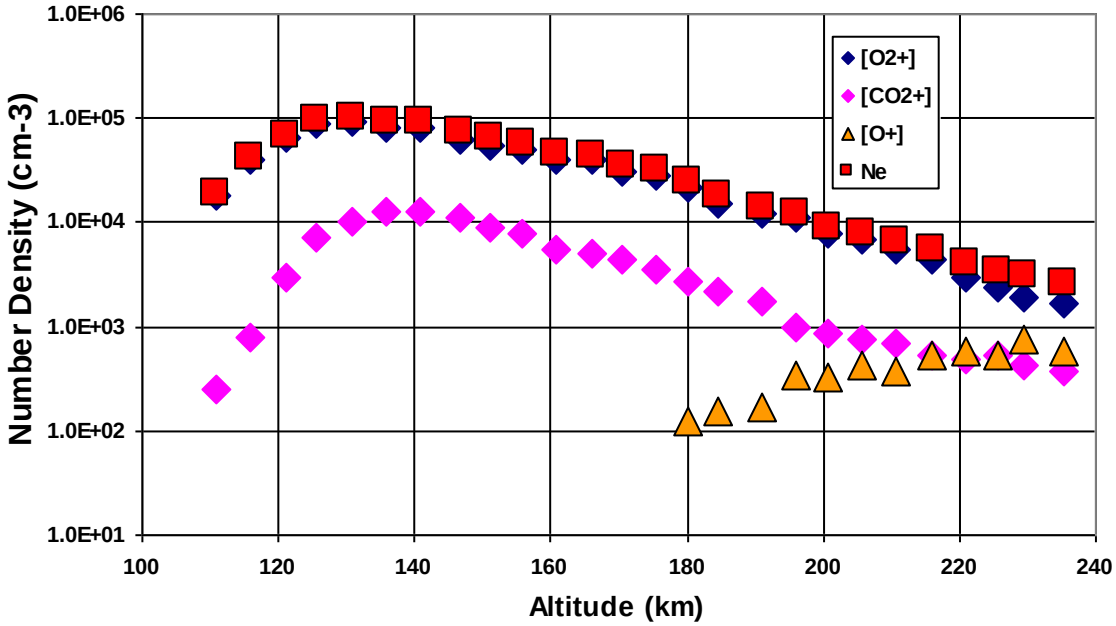

Fig. 5. Measured free stream electron and ion density variation with altitude.

High densities of charged particles are combined with relatively low neutral density, so that in the same altitude range the degree of ionization varies from 0.01 at 200 km to ~10^{-7} at 100 km. Therefore, the free stream conditions

are those of a diluted weakly ionized gas in the state of strong non-equilibrium with the average electron energy exceeding by two orders of magnitude the gas temperature.

Second is the zone of interaction between the entry plasma and the ionospheric gas. Presence of charge particles from the both sides of the shock add to UV radiation from the dense entry plasma and open a new set of processes that contributes to formation of ionization wave behind the shock. In this zone the equilibration of charged particle energy takes place and kinetic description is a valid approach.

For a gas mixture, an appropriate modification to the cross sections of all gas species in the Boltzmann transport equation should be made: $Q_m = \sum_n Q_m^n G^n$ in the first term and $Q_m = \sum_n M Q_m^n G^n / M^n$ and $M = \sum_n M^n G^n$ in the second and third terms. Here Q_m^n is the momentum transfer cross section, G^n is the mole fraction, and M^n is the mass of the molecule of the nth species. We calculated the EEDF by employing a commercial numerical Boltzmann solver, Bolsig+, for weakly ionized gases under steady state conditions [12]. Bolsig+ provides numerical solutions for the EEDF at different values of the reduced electric field (E/N). From the EEDF values we are able to calculate the rate constants (k_j) for certain processes in the MAEP,

$$k_j = \left(\frac{2e}{m}\right)^{1/2} \int_0^\infty \varepsilon Q_j(\varepsilon)\, f(\varepsilon)\, d\varepsilon. \tag{3}$$

The third zone located almost immediately behind the shock is in the charged particle equilibrium and the electron density can be evaluated by using the Saha equation [15],

$$\log \frac{N_e N_{ik}}{N_k - N_{ik}} = -5040 \frac{\varepsilon_k}{T_e} - 1.5 \log \frac{5040}{T_e} + 26.9366 + \log \frac{2 g_{ki}}{g_{k0}}. \tag{4}$$

where N_{ik} is the number density of ions from species k, N_k is the neutral species density, ε_k is the ionization potential of species k, g_{ki} is the statistical weight of the ion species k and g_{k0} is the statistical weight of the neutral species k. In this model we have assumed that the electron temperature (T_e) equilibrates to the gas temperature obtained in Fig. 1. We must also assume that the gas temperature is still high enough that we can neglect the effects of ion chemistry. In addition, we are not including the free stream electron density in this calculation [13].

Since Martian air is composed of many constituents, this calculation is very complex. We observed that the main constituents of the Martian atmosphere are CO_2, N_2, and Ar. During ionization, the major additional neutral species, due to the dissociation of CO_2 and N_2, will be O_2, O, CO, and NO. The number densities of the other neutral species mentioned in the introduction will be negligible in comparison with the densities of the other seven species. As such we have reduced the number of equations needed to find the electron density by assuming that these will be the seven dominant species in the discharge.

We start with an assumed electron density and then calculate N_{ik} from Eq. (4). Then we apply

$$N_e = \sum_k N_{ik} \tag{5}$$

to recalculate the electron density and repeat this process. Due to the fast convergence of this method, we are able to calculate the electron density fairly quickly (see Fig. 6). From the figure we observe that above 50 km the electron density is consistent for each probe. Below there the Pathfinder results are orders of magnitude different from the Viking and MER Opportunity data. It is important to note that the distribution of the electron densities was due to the irregularity in the free stream temperature measurements.

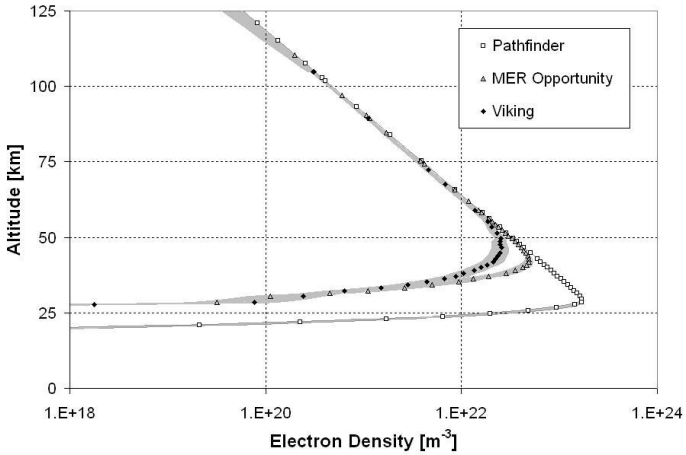

Fig. 6. Calculated values of electron density for MAEP. The shaded regions are due to deviations in the measurement of the free stream temperature data.

IV. Gas Composition

In this work we have used a kinetic model described in Ref. [12] to calculate the gas composition of MAEP. It is based on a system of rate and mass conservation equations formulated by Dinh [14]. The steady state solution for this system can be found by setting the time differentials in each rate equation equal to zero. Including the mass conservation equations, this set of nonlinear coupled equations can be solved for the six unknown concentrations: [CO], [CO_2], [O], [O_2], [O_3], and [O^-]. Fig. 7 shows the dissociation of CO_2 into CO, O, and O_2 under these steady state conditions. We observe from the figure that as the reduced electric field increases to 8.0×10^{-16} V cm^2 over 80% of the CO_2 has been dissociated.

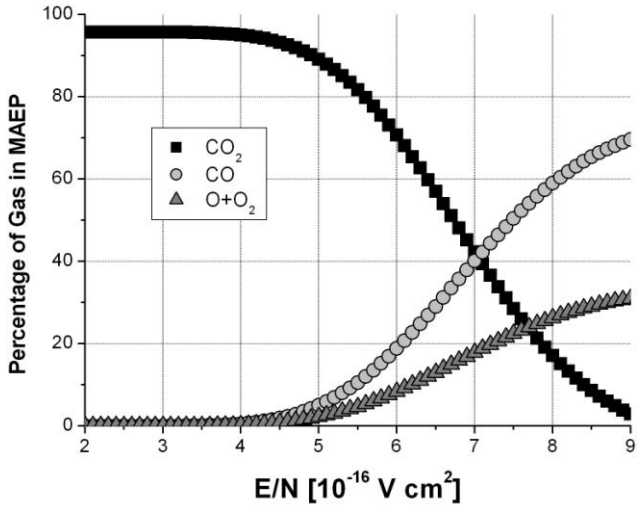

Fig. 7. Dissociation of CO_2 into CO, O, and O_2 in MAEP at an altitude of 40 km.

The reduced electric field (E/N) was estimated as follows. From Fig. 4 we observed that for the Pathfinder data from 10 km – 100 km the total change in jump temperature was approximately 36000 K or 3 eV. We estimate that the total thickness of the shock front is of the order of λ, where λ is the mean free path, or about 0.3 cm. Thus the maximum electric field, E, is approximately 10 V/cm. We determined that the number density, N, was between 2×10^{16} and 1×10^{17} cm^{-3}. Therefore, we estimated the reduced electric field to be in the range of 10 to 60 Td (1 Td ~ 10^{-17} V cm^2).

To calculate the time evolution of the species concentrations, we employed a forth order Runge-Kutta method. This method propagates a solution over an interval h by combining information from several Euler-style steps and then uses this information to match a Taylor series expansion up to $O(h^4)$. Using fixed dissociation rate coefficients,

we made these calculations. In Fig. 8, we observe that about 95% of the CO_2 dissociation was achieved within 6.0×10^{-7} s, which is practically instantaneous even in the time frame of a M = 20 flow. This result is consistent with previous work done by Park *et al.* [5], who showed the dissociation rate for CO_2 is very quick behind the shock front during Martian atmospheric entry.

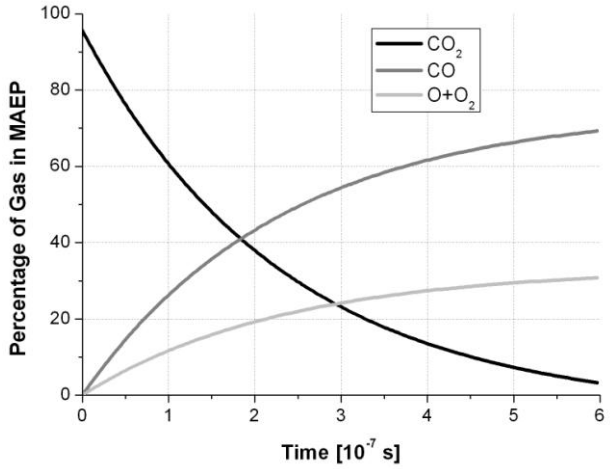

Fig. 8. MAEP composition at $E/N = 5.0 \times 10^{-16}$ V cm^2 and an altitude of 40 km as a function of time.

Changes in gas composition were looked at for various concentrations of CO_2, CO, and O_2 in the mixture. The electron energy distribution function was calculated and these results are presented in Fig. 9. From this figure we can observe how the concentration of CO and O_2 in the mixture changes the distribution function. Therefore, we can conclude that changes in the composition will affect the values of the rate coefficients and concentration of CO_2 over time.

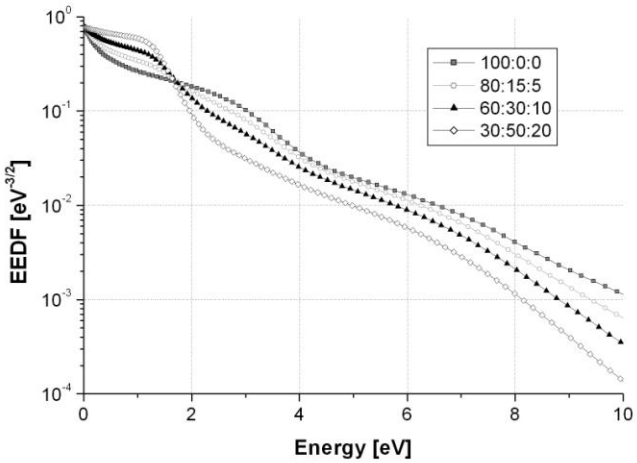

Fig. 9. EEDF of different compositions of CO_2:CO:O_2.

To calculate the composition changes, we started with the initial mixture, and then calculate a new EEDF and corresponding rate coefficients after a selected length of time. A new composition was computed and the corresponding EEDF and rate coefficients were calculated. We used time steps of 0.25×10^{-7} s. As a result of the change in the mixture composition, we observe a decrease in k_{CO2} values over time. This corresponds to a change in the dissociation rate of CO_2 over time, as seen in Fig. 10 where the solid line represents the values that were obtained for constant rate coefficients. Over the same time interval, the percentage of CO_2 dissociation was 15% less.

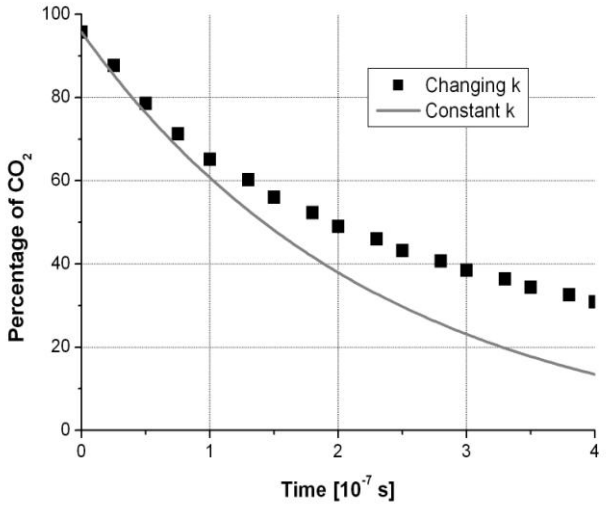

Fig. 10. The change in the percentage of CO_2 at $E/N = 5.0\times10^{-16}$ V cm^2 at an altitude of 40 km as a function of time.

V. Effect of Water Vapor

In the previous sections of the paper, a water-free model was presented. From the literature we found that there is a small amount of water vapor in the atmosphere, 0.03% [9]. The effect of OH radicals from water vapor in the MAEP is summarized in Table 1. To date the altitudinal changes in the concentration of water vapor have not been measured. McElroy *et al.* [15] constructed a photochemical model to compute the concentration for various products of water vapor dissociation in the Martian atmosphere. They found that the concentration of OH molecules peaked at an altitude of about 40 km. However, the calculated density of OH was still less then 0.1% of the total free steam atmospheric density.

TABLE 1. Major reactions due to OH radicals in Martian Atmospheric Entry Plasma.

No.	Reaction	Rate Coefficient	Ref.
1	$CO + OH \rightarrow CO_2 + H$	$k_{10}=1.5\times10^{-13}$ cm^3/s	[16], [17]
2	$O + OH \rightarrow O_2 + H$	$k_{11}=3.0\times10^{-11}$ cm^3/s	[16]
3	$H_2O + e \rightarrow OH + H^-$	$k_{12}=5.0\times10^{-9}$ cm^3/s	[18]

From the last reaction, we observe that the generation rate of OH radicals from the dissociation of water molecules is relatively fast. This indicates that with an electron density of 10^{10} cm^{-3}, the concentration of OH radicals is about 10% of the initial water concentration in the system [14]. The first reaction has a direct effect on the dissociation of CO_2 in the air. Since the amount of water vapor reduces the rate of dissociation, we must take the OH radicals into account in our model. Thus we included an amount of water vapor equivalent to 0.03% of the total gas volume in our model. We observed the changes in the concentration of CO_2 in the atmosphere due to dissociation. In Fig. 11 we observe that with small amounts of water vapor added to the model the dissociation of CO_2 was not effected. However as more water vapor is included in the model, the amount of CO_2 in the MAEP decreased at a slower rate.

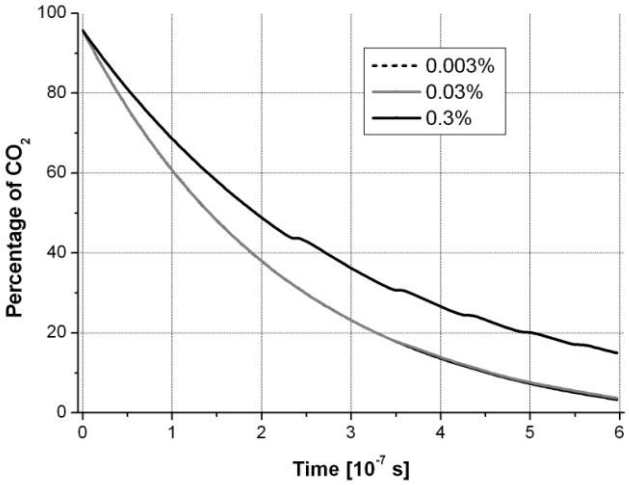

Fig. 11. Percentage of CO_2 in MAEP as a function of time with the amount of water added to the system indicated. The 0.003% curve can not be seen in the figure since it coincides with the 0.03% curve.

Another interesting phenomenon that occurs when water vapor is added to our model is that the production of O_2 in the system increases. As calculated for the Pathfinder Lander, in Fig. 12, we estimated the amount of O_2 in the discharge will increase by about 20% due to the presence of 0.03% of water vapor.

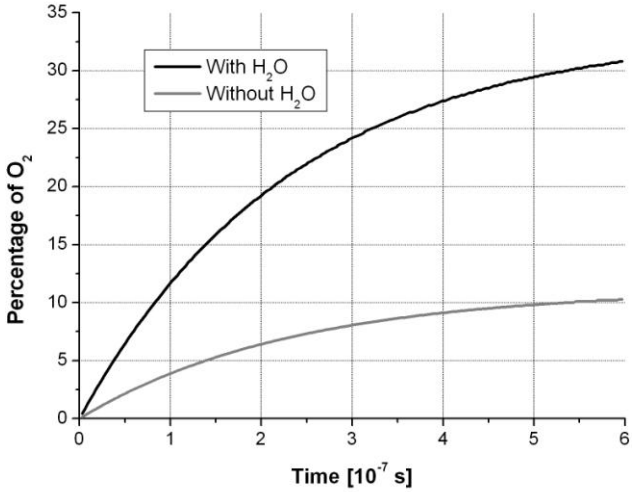

Fig. 12. Percentage of O_2 in MAEP using the Pathfinder Lander data as function of time.

VI. Conclusions

We have described the results of a kinetic model created based on free stream gas temperature, density, and velocity data from the Viking, Pathfinder, and MER Opportunity Landers. Altitudinal distribution of atmospheric composition was taken from Viking data. The density and temperature across the shock front were calculated for each probe. A temperature spread was observed due to the imprecision in the atmospheric models and data for the free stream temperature. The calculated data relies upon the fact that the changes in the composition with altitude are negligible up to 100 km and vary at higher altitudes.

The electron energy distribution function was calculated for the Martian atmosphere by solving the Boltzmann transport equation. For atmospheric gas mixtures, electron temperature and dissociation rate coefficients were then calculated. The electron density was determined from the Saha equation for a simple model with the main species for the ionized gas. From Fig. 6 we saw that above 50 km the electron density was consistent for each probe. At lower altitudes the Pathfinder results were orders of magnitude different from the Viking and MER Opportunity data. In addition, we have shown the variations in electron density when the electron temperature was assumed to be higher or lower than the gas temperature by a factor of two.

A gas composition model was then used to estimate the dissociation of CO_2 in the Martian atmosphere for steady state and non-steady state conditions and a comparison was made. We observed that 95% of the CO_2 was dissociated within 6.0×10^{-7} s assuming that the dissociation rate coefficients were constant in time. However, upon analysis of the change in the rate coefficient with composition, we determined that the amount of CO_2 in the model would be 15% greater in the same time period. By introducing a small amount of water vapor to the model, we found that the rate of dissociation increased with concentrations of water vapor above 0.03% for non-steady state conditions. We also observed an increase in production of O_2 by about 20% due to the presence of 0.03% of water vapor.

References

[1] F. Naderi, D. J. McCleese, and J. F. Jordan, "Mars Exploration", *IEEE Robot. Automat. Mag.*, vol. 13, pp. 72-82, June 2006.

[2] D. F. Doody, "Aerobraking the Magellan spacecraft in Venus orbit," *Acta Astronautica*, vol. 35, pp. 475-480, Jan. 1995.

[3] S. Bougher, G. Keating, R. Zurek, J. Murphy, R. Haberle, J. Hollingsworth, and R. T. Clancy, "Mars Global Surveyor aerobraking: atmospheric trends and model interpretation," *Adv. Space Res*., vol. 23, pp. 1887-1897, Nov. 1999.

[4] V. A. Gorelov, M. K. Gladyshev, A. Yu. Kireev, and S. V. Shilenkov, "Nonequilibrium ionization behind a strong shock wave in the Mars atmosphere," *J. Appl. Mech. Tech. Phys*., vol. 41, pp. 970-976, Nov. 2000.

[5] C. Park, J. T. Howe, R. L. Jaffe, and G. V. Candler, "Review of chemical-kinetic problems of future NASA missions, II: Mars entries," *J. Thermophysics Heat Trans*., vol. 8, pp. 9-23, Jan. 1994.

[6] V. Lago, A. Lebéhot, M. Dudeck, S. Pellerin, T. Renault, and P. Echegut, "Entry conditions in planetary atmospheres: emission spectroscopy of molecular plasma arcjets," *J. Thermophysics Heat Trans.*, vol. 15, pp. 168-175, Feb. 2001.

[7] M. Lino da Silva, F. Passarinho, and M. Dudeck, "Modeling of a CO_2-N_2 plasma flow in a supersonic arcjet facility," *J. Thermophysics Heat Trans*., vol. 20, pp. 680-688, Oct. 2006.

[8] E. Barbosa, B. Lopez, M. Dudeck, A. Kaminska, and B. Izrar, "Numerical simulations of non-equilibrium hypersonic flow in a convergent-divergent nozzle: applications to Mars atmospheric entry simulation," *Proc. 8th International Symposium on Exp. and Comp. Aerothermodynamics of Internal Flows*, Lyon, France, July 2007.

[9] R. G. Prinn and B. Fegley, "The atmospheres of Venus, Earth, and Mars: a critical comparison," *Ann. Rev. Earth Planet. Sci*., vol. 15, pp. 171-212, May 1987.

[10] J. T. Schofield, J. R. Barnes, D. Crisp, R. M. Haberle, S. Larsen, J. A. Magalhaes, J. R. Murphy, A. Seiff, and G. Wilson, "The Mars Pathfinder atmospheric structure investigation/meteorology," *Science*, vol. 278, pp. 1752-1758, Dec. 1997.

[11] D. J. Drake, S. Popović, L. Vušković, and T. Dinh, "Kinetic description of Martian atmospheric entry plasma," *IEEE Trans. Plasma Sci*., in press, 2009.

[12] G. J. M. Hagelaar, and L. C. Pitchford, "Solving the Boltzmann equation to obtain electron transport coefficients and rate coefficients for fluid models," *Plasma Sources Sci. Technol.*, vol. 14, pp. 722-733, Oct. 2005.

[13] R. J. Rosa, *Magnetohydrodynamic Energy Conversion*, New York: McGraw-Hill, 1968.

[14] T. Dinh, "Decomposition of Carbon Dioxide in a Capacitively Coupled Radio Frequency Discharge," Ph. D. dissertation, Dept. of Physics, Old Dominion Univ., Norfolk, VA, 2002.

[15] M. B. McElroy, T. Y. Kong, and Y. L. Yung, "Photochemistry and evolution of Mars' atmosphere: a Viking perspective," *J. Geophys. Res*., vol. 82, pp. 4379-4388, Sept. 1977.

[16] C. Leys, C. V. Egmond, and E. Desoppere, "Dissociation levels in fast-axial-flow CO_2 lasers: A quantitative model," *J. Appl. Phys.*, vol. 78, pp. 2265-2269, Aug. 1995.

[17] W. L. Nighan and W. J. Wiegand, "Influence of negative-ion processes on steady-state properties and striations in molecular gas discharges," *Phys. Rev. A*, vol. 10, pp. 922-945, Sept. 1974.

[18] D. A. Parkes, "Negative ion reactions in nitrous oxide+ carbon dioxide mixtures," *J. Chem. Soc., Faraday Trans. 1*, vol. 68, pp. 2121-2128, 1972.